AIMS Materials Science, 4(3): 738-754.
DOI: 10.3934/matersci.2017.3.738
Received: 25 April 2017
Accepted: 07 June 2017
Published: 13 June 2017

http://www.aimspress.com/journal/Materials

Research article

Preparation of gold-containing binary metal clusters by co-deposition-precipitation method and for hydrogenation of chloronitrobenzene

Ya-Ting Tsu [1] and Yu-Wen Chen [1,2,*]

[1] Department of Chemical and Materials Engineering, National Central University, Jhong-Li 32001, Taiwan
[2] Department of Chemistry, Tomsk State University, Tomsk, Siberia, Russia

* **Correspondence:** Email: ywchen@cc.ncu.edu.tw; Tel: +886-3-4227151 ext. 34203; Fax: +886-3-4252296.

Abstract: Nano-gold catalyst has been reported to have high activity and selectivity for liquid phase hydrogenation reaction. In this study, gold-containing bimetals were loaded on TiO_2. For bimetallic catalysts, gold and different metals were prepared by the deposition-precipitation method, and then used $NaBH_4$ to reduce metal cations. The catalysts were characterized by X-ray diffraction, transmission electron microscopy, high resolution transmission electron microscopy, and X-ray photoelectron spectroscopy. The catalytic properties of these catalysts were tested by hydrogenation of p-chloronitrobenzene (p-CNB) in a batch reactor at 1.1 MPa H_2 pressure, 373 K and 500 rpm. Cu, Ag, Ru, and Pd formed nano-alloy with Au. In addition, Cu–Au, Ag–Au, and Ru–Au alloy had Cu-, Ag-, and Ru-enriched surface, respectively. Instead, Pd–Au alloy had Pd-enriched surface. There are two kinds of alloy effects: (1) geometric effects, i.e., the surface-enriched metal would change the distance of Au–Au atoms that is required for facilitating the hydrogenation of chloronitrobenzene; and (2) electronic effects, which involve charge transfer between the metals. The activity decreased in the following order: $PdAu/TiO_2$ > Au/TiO_2 > $NiAu/TiO_2$ > $AgAu/TiO_2$ > $RuAu/TiO_2$ > $CuAu/TiO_2$. Comparing with other metals, adding Pd in Au showed a higher activity. Adding palladium could reduce gold-valence state, and increased active sites for reaction.

Keywords: nanoalloy gold catalyst; metal cluster; titanium oxide; hydrogenation; chloronitrobenzene

1. Introduction

Since Bond et al. [1,2] studied the hydrogenation of olefins over supported gold catalyst and Haruta [3] successfully prepare gold nano-clusters on reducible support as a catalyst on the low temperature of oxidation CO reaction, nano-gold has been found to be a good catalyst in numerous reactions. Because of its superior ability of hydrogenation adsorption, gold catalyst has many potential advantages of competitive selectivity and activity on hydrogenation reactions [4–31]. Hydrogenation over gold catalysts exhibits structure sensitivity, where smaller particles (less than 10 nm) deliver higher activities. In other words, gold activates hydrogen, provide it is present as nano-sized particles, which are generally stabilized on a support [25,31–35]. Molecular hydrogen does not chemisorb on bulk gold [15] but weakly interacts at 78 K, desorbing with temperature at 125 K [36]. Instead, dissociative chemisorption of H_2 occurs on low-coordinated Au sites, such as edges and corners [37].

Bimetallic nanoparticles with well-defined structures, compositions, and shapes have wide attention in catalysis study due to dramatically improved catalytic performances compared to monometallic nanoparticles [38–41]. There are two kinds of alloy effects: (1) geometric effects, i.e., a finite number of atoms in a particular geometric orientation that are required for facilitating a particular catalytic process; and (2) electronic effects, which involve charge transfer between the metals or orbital rehybridization of one or both metallic components. A significant development in catalysis for gold has seen the use of Au based alloys because it has fine selectivity and activity on reactions [42–51]. Bimetallic catalysts have attracted extensive attention because of their different properties from either of the constituent metals, and often enhanced catalytic stabilities, activities and/or selectivities. The addition of a second metal can favor the reduction of first, increase the dispersion of a metal which has a tendency to form large particles or decrease its fritting [43–47]. The gold-based bimetallic catalysts were applied on several reactions in industry because of its particular ability of product selectivity. For instance, Nutt et al. [46] used Pd–Au bimetallic nanoparticle catalysts for aqueous-phase trichloroethene hydrodechlorination reaction. Piccinini et al. [50] used direct synthesis of hydrogen peroxide by Au–Pd/TiO_2 catalyst. Yuan et al. [52] studied Ni–Au alloy catalysts for application in catalytic hydrodechlorination. Cárdenas-Lizana et al. [31] used Au–Ni alloy catalysts on gas phase hydrogenation reaction. Au–Cu/TiO_2 was used for partial oxidation of methanol reaction [53].

Hydrogenation of halonitroaromatics to the corresponding haloamines is a formidable challenge, which has several satisfactory solutions and has been industrialized on a large scale. Comparing with the traditional synthesis routes, the selective hydrogenation of halonitroaromatics to the corresponding haloamines was superior in saving resources, reducing the waste disposal and protecting the environment [54–57]. However, the hydrogenation of halonitrobenzene was very complex, and the overall reaction mechanism is shown in Scheme 1. The nitro group could be hydrogenated to amine group to produce *p*-chloroaniline (*p*-CAN) from the hydrogenation of *p*-chloronirobenzene (*p*-CNB). Then, it might be further hydrogenated to aniline (AN) and the chlorine atom might be eliminated in hydrogenation to form nitrobenzene (NB). Furthermore, NB could be hydrogenated to AN. In general, dechlorination could proceed in all reaction steps, especially, after reaching a stoichiometric consumption of hydrogen.

Regarding to the mechanism, the metal atoms existing on the surface of catalyst is favorable for the activation of polar N=O bond in $–NO_2$ group, then the dissociated H atoms near the activated

N=O bond attacks the N=O bond. Thus, the nitro group is reduced to $–NH_2$ group. The weak interaction among metal, catalyst, and $–NH_2$ will shorten the residence time on the surface of catalysts, so the dehalogenation of C–Cl bond is weakened [56]. It has been reported that the gas phase hydrogenation of *p*-chloronitrobenzene over Au supported on alumina and titania [31] was 100% selective in terms of $–NO_2$ group reduction to *p*-chloroaniline over a prolonged (up to 80 h) time on-stream. However, the reaction condition in liquid phase is different from that in gas phase reaction.

The aim of this study was to prepare the gold-containing bimetallic catalysts which could be applied for *p*-CNB hydrogenation in liquid phase reaction. A series of M (Cu, Ni, Ag, Ru, Pd)–Au/TiO_2 catalysts were prepared and tested. The catalysts were characterized by X-ray diffraction (XRD), transmission electron microscopy (TEM), and X-ray photoelectron spectroscopy (XPS).

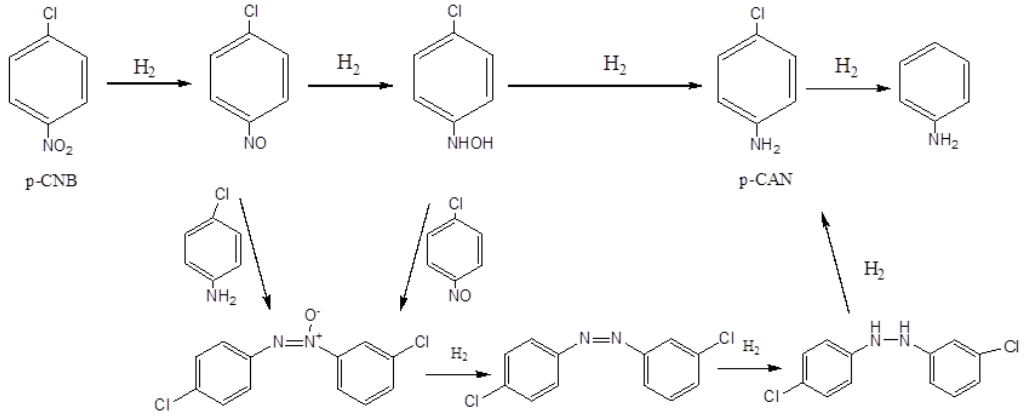

Scheme 1. Reaction route for hydrogenation of *p*-CNB.

2. Materials and Method

2.1. Chemicals

Reagents used in this study were analytical grade. TiO_2 was purchased from Evonik (P-25). $Pd(NO_3)_2$ (Alfa Aesar, 99.9%) was used as the precursor for loading palladium by co-deposition-precipitation. $HAuCl_4$ (Showa, 99.0%) was used as the precursor for loading gold by co-deposition-precipitation method. NH_4OH (Showa) was used as neutralizers to adjust the pH value of preparation. Sodium borohydride (>98%) was purchased from Alfa Aesar. The reactant, p-chloronitrobenzene was from Acros (Belgium). High purity hydrogen gas (>99.99%) was derived from Air Product and used without any further purification.

2.2. Preparation of Catalysts

Bimetallic gold-containing cluster catalysts were prepared with different metal precursors on TiO_2 support by co-deposition-precipitation method [58,59]. Au metal loading was fixed at 3 wt.%. The Au/M molar ratios of various catalysts are listed in Table 1. $HAuCl_4$ solution and second metal

precursor were prepared and dropped into the aqueous solution of TiO_2 support under stirring. The temperature was maintained at 65 ℃, and the pH was adjusted to 7 with 1 M NH_4OH. After aging for 2 h, $NaBH_4$ solution was added into the aqueous solution and stirred for 10 min to reduce both metal cations. The precipitate was filtered and washed with hot water (65 ℃) until no Cl^- was detected with $AgNO_3$ solution. The filter cake was grounded and dried at 40 ℃ overnight.

Table 1. The Au/M ratio of bimetallic catalysts (Au loading was 3 wt.%).

Catalyst	Au/M (molar ratio)
Au/TiO_2	
$CuAu/TiO_2$	4:1
$RuAu/TiO_2$	3:1
$NiAu/TiO_2$	3:1
$AgAu/TiO_2$	3:1
$PdAu/TiO_2$	3:1

2.3. Characterization of Catalysts

The as-prepared samples were dried under the vacuum condition before carrying out the analysis of X-ray diffraction (XRD), transmission electron microscopy (TEM), and X-ray photoelectron spectroscopy (XPS).

2.3.1. XRD

The XRD instrument type was Siemens D500 powder diffractometer. The XRD patterns were collected by using Cu $K_{\alpha 1}$ radiation (0.15405 nm) at a tube voltage and current of 40 kV and 20 mA, respectively. The samples for XRD were prepared as thin layers on the sample holder and scanned over the range of 2θ = 20–70 ° at the rate of 0.05 ° s^{-1} to identify the crystalline structure.

2.3.2. TEM

The morphologies and particle size of the samples were determined by TEM (Jeol JEM-2000 FX II). The operation was at 120 kV. The TEM samples were prepared as following. A small amount of powder was put into the sample bottle filled with 99.8% methanol solvent. After agitating under ultrasonic environment for 90 min, one drop of the dispersed slurry was dipped onto a carbon coated copper mesh (300#; Ted Pella Inc., CA, USA) and dried in vacuum over night.

2.3.3. XPS

The XPS spectra were recorded with a Thermo VG Scientific Sigma Probe spectrometer. The XPS spectra were collected by using Al K_α radiation at a voltage and current of 20 kV and 30 mA respectively. The base pressure in the analyzing chamber was maintained in the order of 10^{-9} torr and the spectrometer was operated at 23.5 eV pass energy. The sample was sputtered using Ar^+ ions for 15 min to remove the oxidation parts which were formed during the XPS operation. All the binding

energies were calibrated by using the contaminant carbon (C 1s = 284.5 eV). Peak fitting was done by using the software, XPSPEAK 4.1 with Shirley background, 30:70 Lorentzian to Gaussian convolution product shapes.

2.4. Hydrogenation Reaction

The catalytic activities and selectivities of the samples were tested by the liquid-phase hydrogenation of *p*-CNB. All the experiments were carried out in the cylindrical stirred-tank reactor (Parr Instrument Model 4842) with 160 mL capacity. A four-bladed pitched impeller was placed for effective agitation and the agitator was connected to an electric motor with variable speed which was up to 1700 rpm. A pressure transmitter and an automatic temperature controller were also provided. The gases were supplied from cylinders and introduced to the base of reactor. The reactor was charged by 0.5 g catalyst and 2.54 g *p*-CNB in 80 mL methanol solvent, the concentration of *p*-CNB was 0.2 M. In the beginning, air was flushed out of the reactor by hydrogen at room temperature. After the designated temperature was reached, hydrogen was fed to reach the preset pressure and the stirring speed was fixed at 500 rpm. These conditions were maintained throughout the reaction, defining this point as time zero. During the reaction run, the samples were withdrawn periodically and analyzed by a gas chromatograph equipped with a flame ionization detector and a 3 m × 1/8 inch stainless steel column packed with 5% OV-101 on Chromsorb WAW-DMSC (80–100 mesh). The experiments have been repeated twice at least and the reproducibility was above 98%.

The conversion and the selectivity to each product were calculated as following:

$$Conversion\,(\%) = \left(1 - \frac{C_{p-CNB}}{C_{AN} + C_{NB} + C_{p-CAN} + C_{p-CNB}}\right) \times 100\% \tag{1}$$

$$S_{AN}(\%) = \left(\frac{C_{AN}}{C_{AN} + C_{NB} + C_{p-CAN}}\right) \times 100\% \tag{2}$$

$$S_{NB}(\%) = \left(\frac{C_{NB}}{C_{AN} + C_{NB} + C_{p-CAN}}\right) \times 100\% \tag{3}$$

$$S_{p-CAN}(\%) = \left(\frac{C_{p-CAN}}{C_{AN} + C_{NB} + C_{p-CAN}}\right) \times 100\% \tag{4}$$

where C_{AN}, C_{NB}, $C_{p\text{-}CAN}$ and $C_{p\text{-}CNB}$ represented the concentrations of aniline, nitrobenzene, *p*-chloroaniline and *p*-chloronitrobenzene, respectively.

3. Results and Discussion

3.1. XRD

The XRD patterns of gold-containing bimetallic catalysts are shown in Figure 1. These catalysts only showed intense TiO_2 peaks, including anatase phase at 2θ = 25.06 °(101), 38.14 °(004), 48.03 °

(200) and 54.15 ° (105) and rutile phase 2θ = 27.50 ° (110), 36.11 ° (101), and 55.18 ° (211), as expected since TiO_2 was from Evonik P-25. No distinct gold peaks at 2θ = 38.2 ° and 44.5 ° and no other metal peaks were observed, since the gold-containing bimetallic cluster size was too small to detect. This confirms that the size of bimetallic clusters were less than 4 nm.

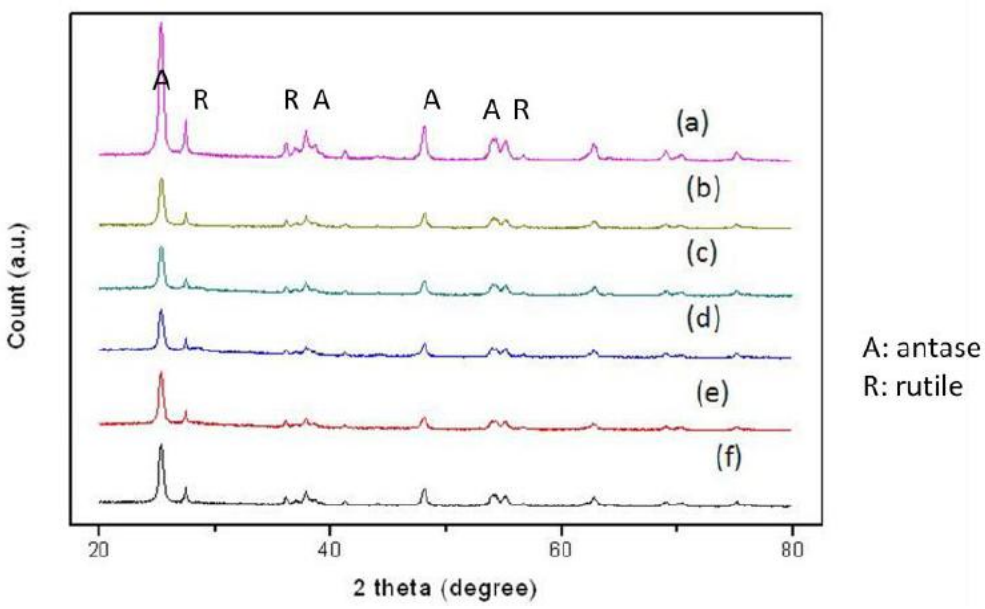

Figure 1. XRD patterns of the catalysts, (a) Au/TiO_2, (b) $NiAu/TiO_2$, (c) $CuAu/TiO_2$, (d) $RuAu/TiO_2$, (e) $PdAu/TiO_2$, and (f) $AgAu/TiO_2$.

3.2. TEM

The TEM images of gold-containing bimetallic catalysts are shown in Figure 2. One can see that there were many small bimetallic particles in each sample, and the average particle size was 2.0–3.5 nm. The average particle size, $d_{particle}$, was calculated using the following equation: $d_{particle} = \Sigma n_i di_i^3/\Sigma n_i d_i^2$, where n_i is the number of particles of diameter $d_{particle}$. The particle size of TiO_2 P-25 from Evonik was in the range of 20–40 nm. The sizes of gold-containing bimetallic particles were around 2–4 nm as shown in Table 2. The results are in agreement with XRD results. There is no significant difference among all samples, indicating that the co-deposition-precipitation method can be used to prepare bimetallic clusters on TiO_2 support.

Table 2. Average sizes of gold-containing bimetallic particles.

Sample	Average size (nm)
Au/TiO_2	3.3
$CuAu/TiO_2$	2.9
$RuAu/TiO_2$	1.9
$NiAu/TiO_2$	2.0
$AgAu/TiO_2$	2.7
$PdAu/TiO_2$	2.1

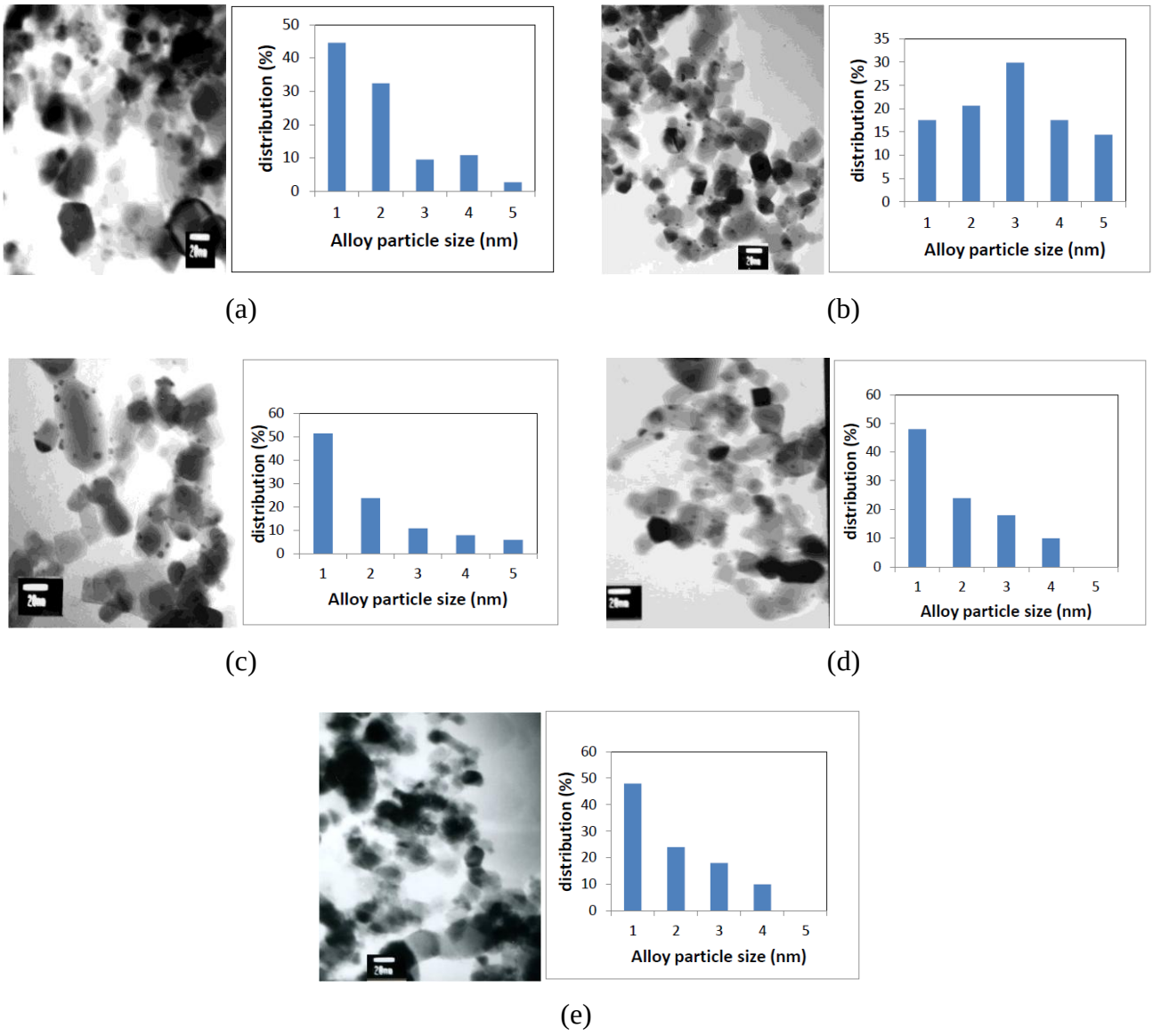

Figure 2. TEM images of (a) $AgAu/TiO_2$, (b) $CuAu/TiO_2$, (c) $PdAu/TiO_2$, (d) $NiAu/TiO_2$, and (e) $RuAu/TiO_2$.

3.3. XPS

The compositions and electronic state of each species on the surface of the samples were determined by XPS analysis. All metals were deposited on TiO_2 support. Since the isoelectric point of TiO_2 is around 8, so the pH value during deposition precipitation process should be lower than 8. If the pH value is too high, the particle size would be big. If the pH value is too low, only very small amount of metal would deposit on the support. Therefore the pH value was controlled at 7 in this study. The temperature was controlled at 65 ℃.

The XPS spectra of Au 4f, Ti 2p and O 1s in the different bimetallic catalysts are shown in Figures 3–5. The XPS spectra for all the catalysts suggest that Au species existed in different states as metallic gold (Au^0) and Au^{3+}. Au 4f was characterized by the doublet of two spin orbit components, viz., Au $4f_{7/2}$ and Au $4f_{5/2}$ [51]. The peaks for metallic gold located at 84.0 eV (Au $4f_{7/2}$)

and 87.7 eV (Au $4f_{5/2}$). The peaks for Au^{3+} were centered at 86.3 eV (Au $4f_{7/2}$) and 89.6 eV (Au $4f_{5/2}$). The Ti 2p XPS spectrum was deconvoluted into four peaks , which Ti $2p_{3/2}$ at 455 ± 0.3 eV is indicative as Ti^{2+}, whereas Ti $2p_{3/2}$ at 459 eV is indicative as Ti^{4+}. It should be noted that all bimetals were alloy with nano size. In the nanosize range, the surface concentrations were different among various samples. Cu, Ag, Ru, and Pd would form nano-alloy with Au [60–64]. In addition, Cu–Au, Ag–Au, and Ru–Au alloy would have Cu-, Ag-, and Ru-enriched surface, respectively [62,63,64]. Instead, Pd–Au alloy would have Pd-enriched surface [60,61]. There are two kinds of alloy effects: (1) geometric effects, i.e., the surface-enriched metal would change the distance of Au–Au atoms that is required for facilitating the hydrogenation of chloronitrobenzene; and (2) electronic effects, which involve charge transfer between the metals.

The O 1s XPS spectrum was deconvoluted into two peaks as shown in Figure 5. The O 1s peak at ~529 eV was indicative of metal oxides (O^{2-}), whereas the peak at ~531 eV was indicative of hydroxides (OH^-). As shown in Figure 5, the peak of Au show that only $PdAu/TiO_2$ had positive shift, and other bimetallic Au peaks had negative shift. This result indicates that each different metal interacted with gold in different ways. In this series of catalysts, the Ti 2p peaks were only existed as Ti^{4+} peaks as shown in Figure 4. The O 1s peaks of all the samples showed a few amount of OH^- in Figure 5 and Table 3.

Table 3 lists the binding energies of various species of $M–Au/TiO_2$ catalysts. The Au binding energy shifted negatively in $AgAu/TiO_2$, $NiAu/TiO_2$, $RuAu/TiO_2$, and $CuAu/TiO_2$, whereas Au binding energy shifted positively only in $PdAu/TiO_2$. The Ti 2p peaks had some negative shift from 459 eV. However, the binding energy of O 1s peak did not show obviously shift. The chemical compositions of Au, Ti and O on surface of each sample are tabulated in Table 4. Besides, the widths of the Au peaks in bimetallic samples were broader than that of monometallic one, due to the interactive effect of gold and second metal.

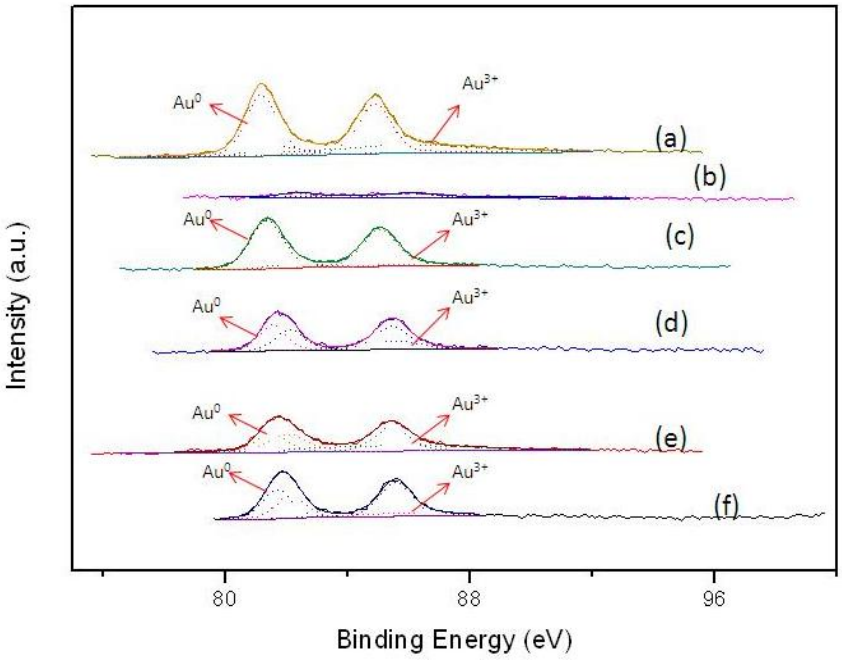

Figure 3. XPS spectra of Au 4f for (a) Au/TiO_2, (b) $RuAu/TiO_2$, (c) $CuAu/TiO_2$, (d) $AgAu/TiO_2$, (e) $PdAu/TiO_2$, and (f) $NiAu/TiO_2$.

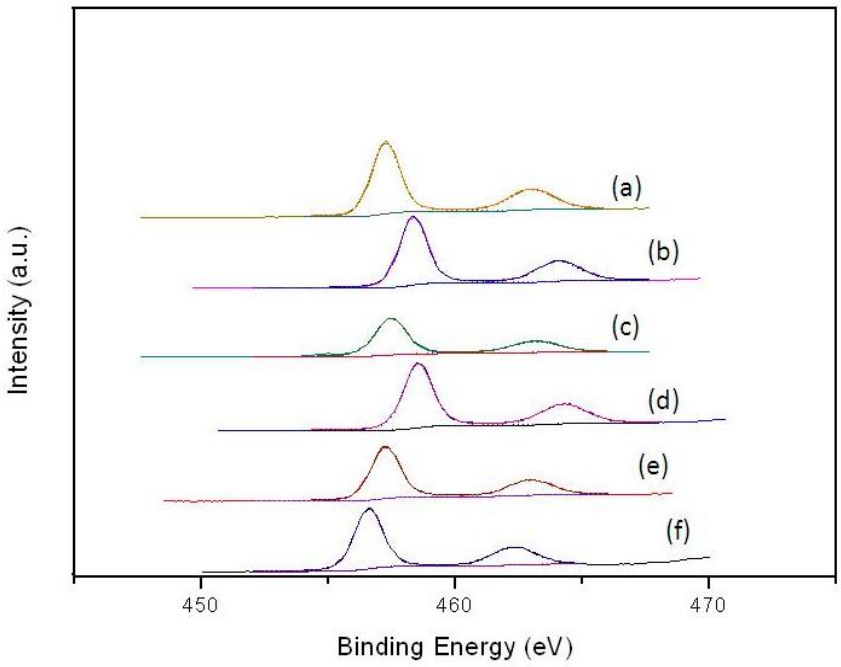

Figure 4. XPS spectra of Ti 2p for (a) Au/TiO_2, (b) $AgAu/TiO_2$, (c) $PdAu/TiO_2$, (d) $RuAu/TiO_2$, (e) $CuAu/TiO_2$, and (f) $NiAu/TiO_2$.

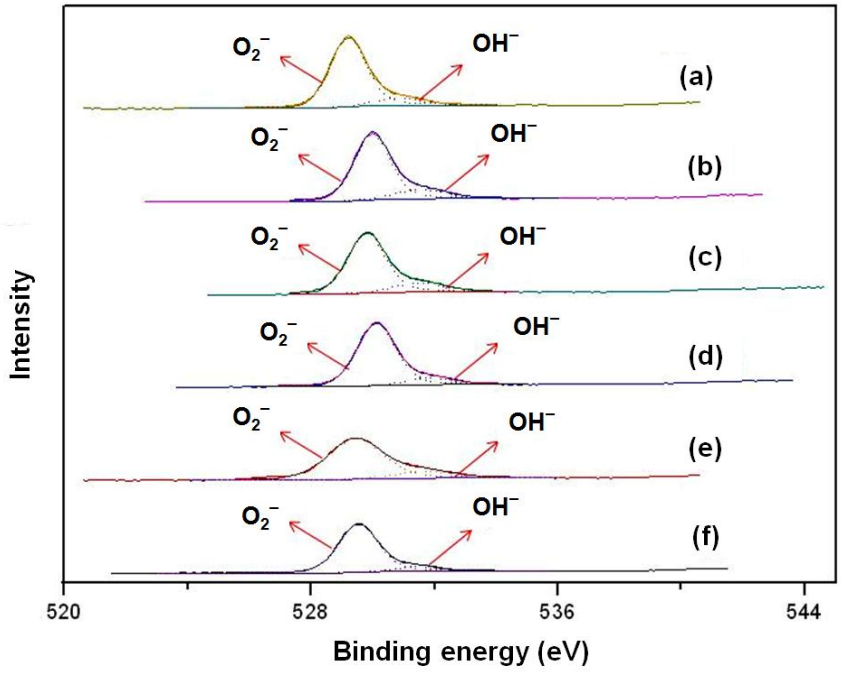

Figure 5. XPS spectra of O 1s for (a) Au/TiO_2, (b) $AgAu/TiO_2$, (c) $NiAu/TiO_2$, (d) $RuAu/TiO_2$, (e) $PdAu/TiO_2$, and (f) $CuAu/TiO_2$.

Comparing with monometallic gold on TiO_2, the peaks of Au in bimetallic samples had 0.2–0.3 eV shift as shown in Figure 3. According to the literature [65], the shift of Au peaks is due to

the second metal interacting with Au and become partial surface alloy formation. In this series of bimetallic catalyst, the second metal became partial oxidation ($M \rightarrow M^{n+}$) as induced by gold.

Table 3. Analysis of the binding energy of the species on the surface of the catalyst.

catalyst	Au $4f_{7/2}$		Ti $2p_{3/2}$		O 1s	
	Au^0 (eV)	Au^{3+} (eV)	Ti^{2+} (eV)	Ti^{4+} (eV)	O^{2-} (eV)	OH^- (eV)
Au/TiO_2	84.88	85.74		457.25	529.20	530.81
$AgAu/TiO_2$	81.53	82.10		458.34	529.98	531.54
$NiAu/TiO_2$	81.699	82.14		456.58	529.8	531.49
$CuAu/TiO_2$	81.36	82.29		457.24	529.53	531.38
$RuAu/TiO_2$	82.33	84.03		458.53	530.11	531.85
$PdAu/TiO_2$	85.40	85.44		457.44	529.44	531.66

Table 4. Analysis of the compositions of the species on the surface of the catalyst.

catalyst	Au $4f_{7/2}$		Ti $2p_{3/2}$		O 1s	
	Au^0 (%)	Au^{3+} (%)	Ti^{2+} (%)	Ti^{4+} (%)	O^{2-} (%)	OH^- (%)
Au/TiO_2	65.71	34.29		100	88.39	11.61
$AgAu/TiO_2$	59.26	40.74		100	84.51	15.49
$NiAu/TiO_2$	38.39	61.61		100	83.65	16.35
$CuAu/TiO_2$	89.5	10.5		100	91.84	8.16
$RuAu/TiO_2$	46.35	53.65		100	89.6	10.4
$PdAu/TiO_2$	49.91	50.09		100	85.52	14.48

3.4. Hydrogenation Reaction

The conversion of *p*-CNB vs. reaction time on stream over various catalysts is shown in Figure 6. The main product of *p*-CNB hydrogenation was *p*-CAN and there were two by-products, NB and AN. In each case, the concentration of NB and AN increased in the initial period, then NB decreased and *p*-CAN and AN increased. The reaction scheme can be simplified to scheme 2. There are two interpretations for these results: one is that the rate of hydrogenation carried on the path (1) is faster than that of path (3); another is that *p*-CNB mainly followed path (1) then path (2), but less path (3) and path (4). However, the increasing rate of aniline was not obvious, so the possibility of the first case was low.

The reaction was first order with respect to the concentration of *p*-CNB. As shown in Figure 6, the activity of $PdAu/TiO_2$ catalyst showed better performance than the other catalysts. In the gold-based bimetallic catalysts, $PdAu/TiO_2$ had the highest reaction rate, its conversion of *p*-CNB reached 100% within 20 min. The activities of the catalysts decreased in the following order: $PdAu/TiO_2 > Au/TiO_2 > NiAu/TiO_2 > AgAu/TiO_2 > RuAu/TiO_2 > CuAu/TiO_2$ as shown in Figure 6. It could be concluded that Pd and Au mixed as nano-alloy and Pd modified gold to become a very active site on the catalyst for hydrogenation of *p*-CNB. Although the selectivity of *p*-CAN on $PdAu/TiO_2$ was lower than other catalysts, the yield of p-CAN on $PdAu/TiO_2$ was higher than other

catalysts since its activity was much higher than other samples.

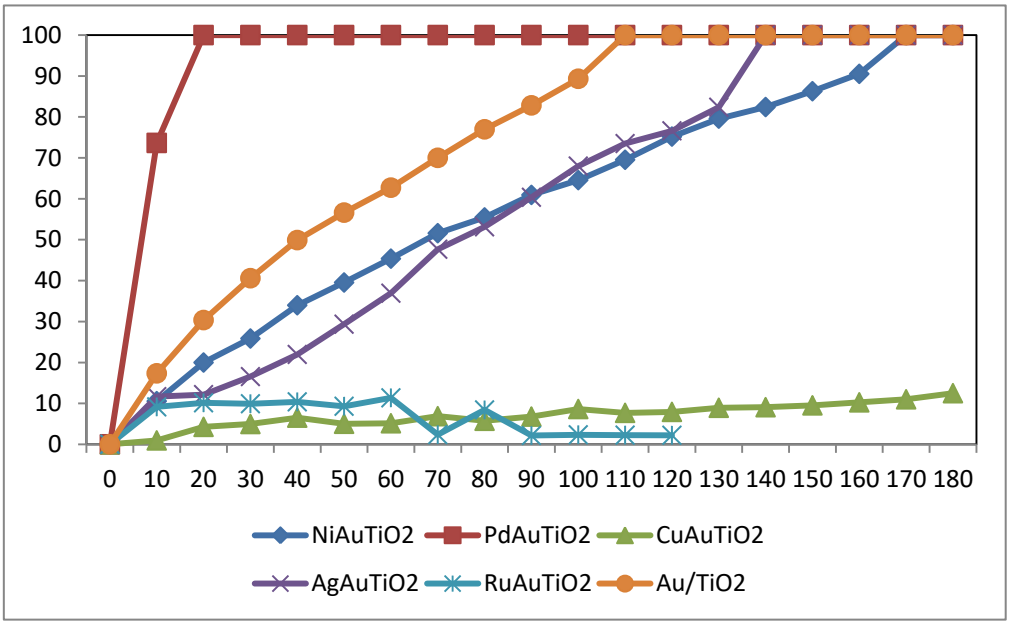

Figure 6. *p*-CNB conversion vs. reaction time on M-Au/TiO_2 catalysts.

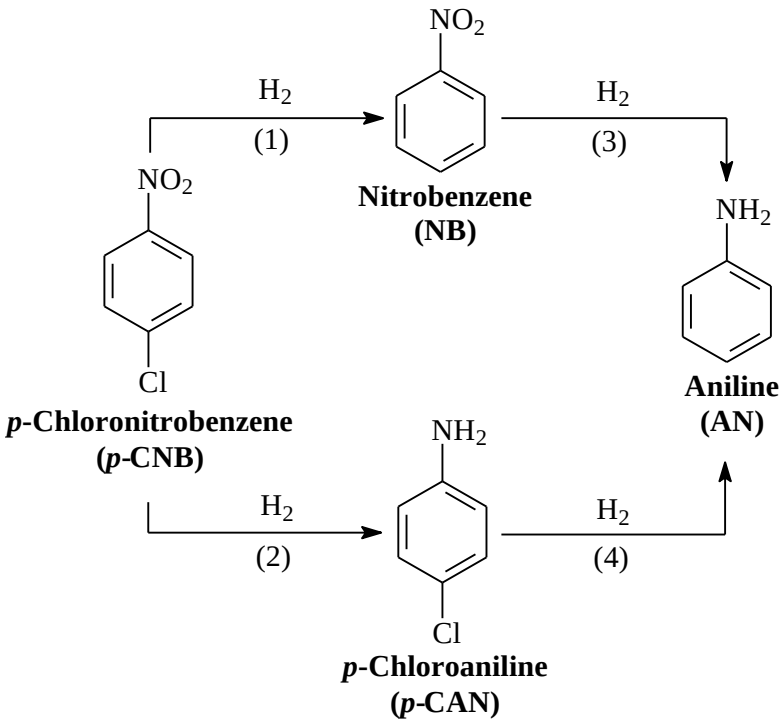

Scheme 2. Simplified reaction scheme.

Based on the electronic effect, both –NO_2 and –Cl adsorb strongly on electron-rich metal, which would result in higher activity in the hydrogenation of the nitro group and dechlorination. There are

two highly electronegative elements, N and O existing in the nitro group. Oxygen atom is more electronegative than nitrogen atom; hence, the N–O bond is polarized. The partially positive charge of nitrogen atom, combined with high electronegativity, led to the nitro group being easily reduced. Because of the combination of inductive and resonance effects, the para-substituted nitro group has high electronegativity. About chorine, only the inductive effect is present. Since the $–NO_2$ group is more electronegative than –Cl, $–NO_2$ is supposed to occupy the active site on the gold particles at the start of the reaction. Owing to the chemical bonding in the nitro group, the nitrogen atom is positively charged and each oxygen atom has a partial negative charge, and the nitro group strongly attracts electrons. For this reason the TiO_2 as a support has great ability of donating electron to gold, the gold on the surface becomes more electron-enriched. Moreover, the different metal mixed with gold could reduce gold and form gold-based nano-alloy particles. The high electronegativity of $–NO_2$ would be adsorbed on electron-enrich gold, which would result in higher activity in the hydrogenation of the nitro group and dechlorination. The electron density of $PdAu/TiO_2$ was higher than those of other catalysts, which could lead into higher reaction activity. In the hydrogenation of *p*-CNB, since part of electron transferred to gold facilitated the catalyst attracting the partial negative oxygen easily so the N=O bond of $–NO_2$ group was activated, and the hydrogen could attack the partial positive nitrogen easily.

3.5. Reaction Rate Constant

The hydrogenation reaction rate constant was calculated for all gold catalysts. Based on the conversion-time curves in the hydrogenation of *p*-CNB (Figure 6), it indicates that the reaction was first order with respect to the concentration of *p*-CNB. The reaction rate can be expressed as following:

$$-r_A = kC_{A0} \cdot (1 - X_A) \tag{5}$$

where k is reaction rate constant, s^{-1}; C_{A0} is the initial concentration of reactant; and X_A is conversion, %. The reaction was carried out in a constant-volume batch reactor, so:

$$-r_A = C_{A0} \frac{dX_A}{dt} \tag{6}$$

where t is reaction time, s. Combined these two equations by using integral method of analysis of data, one could get:

$$-\ln(1 - X_A) = kt \tag{7}$$

A plot of $-\ln(1 - X_A)$ vs. t could derive the slope which represents the reaction rate constant. Because of the induction period appeared in the initial stage of reaction, the data in initial stage was neglected. The results are listed in Table 5. As expected, the rate constant of $PdAu/TiO_2$ was the highest among all catalysts in this study.

Table 5. Effect of additive on the hydrogenation of *p*-CNB over M–Au/TiO_2.

catalysts	Conversion (%)	Selectivity (%)			reaction rate constant (s^{-1})	reaction rate: [mol *p*-CNB/ (g metal × s)]	reaction rate [mol *p*-CNB/ (mol metal × s)]
		p-CAN	AN	NB			
NiAu/TiO_2	100	98.92	0.96	0.12	0.0086	0.00017	0.0275
PdAu/TiO_2	100	84.01	15.99	0	0.1344	0.001524	0.265
CuAu/TiO_2	12.5	92.33	0	7.67	0.0008	0.000034	0.0057
AgAu/TiO_2	100	100	0	0	0.0112	0.000177	0.0308
RuAu/TiO_2	2.2	0	0	100	0.0045	0.00014	0.0242

4. Conclusion

A series of gold-based bimetallic catalysts were prepared by co-deposition-precipitation method, where the second metals were Ag, Ru, Ni, Pd, and Cu, respectively. They were characterized by X-ray diffraction, transmission electron microscopy and X-ray photoelectron spectroscopy. The catalytic properties of the catalysts were tested by the liquid phase hydrogenation of *p*-CNB at 373 K and 1.1 MPa H_2 pressure.

No distinct metal XRD peaks were observed because the metal particles were too small to detect, and only the peaks of TiO_2 were found. The TEM images showed that the average gold-metal alloy particle size were less than 4 nm, in consistent with the XRD results. Using deposition-precipitation method, one was successfully prepare alloy-cluster on TiO_2 support. The XPS spectra showed the gold peaks shifted in various samples, depending on the species of second metal. Only the Au peak in PdAu/TiO_2 shifted positively. The Au peaks in other samples had negative shift. Furthermore, the width of gold peaks became broader owing to the formation of gold-based alloy particles. Au was enriched on the surface of Pd–Au particles. Ni–Au, Cu–Au, Ag–Au and Ru–Au had different behavior, i.e., the second metals were surface-enriched on these samples. Both ensemble and electronic effects of alloy clusters modified the catalytic performance of the catalysts, resulting in different activity and selectivity in hydrogenation of *p*-CNB to *p*-CAN. The activity decreased in the following order: PdAu/TiO_2 > Au/TiO_2 > NiAu/TiO_2 > AgAu/TiO_2 > RuAu/TiO_2 > CuAu/TiO_2. PdAu/TiO_2 had the highest reaction rate among all catalysts, its conversion of *p*-CNB reached 100% within 20 min.

Conflict of Interest

The authors declare that there is no conflict of interest.

References

1. Bond GC, Sermon PA, Webb G, et al. (1973) Hydrogenation over supported gold catalysts. *J Chem Soc Chem Commun* 444–445.
2. Bond GC, Thompson DT (1999) Catalysis by gold. *Catal Rev* 41: 319–388.
3. Haruta M, Kobayashi T, Sano H, et al. (1987) Novel gold catalysts for the oxidation of carbon monoxide at a temperature far below 0 ℃. *Chem Lett* 16: 405–408.

4. Bailie JE, Hutching GJ (1999) Promotion by sulfur of gold catalysts for crotyl alcohol formation from crotonaldehyde hydrogenation. *Chem Commun* 2151–2152.
5. Pawelec B, Cano-Serrano E, Campos-Martin JM, et al. (2004) Deep aromatics hydrogenation in the presence of DBT over Au–Pd/γ-alumina catalysts. *Appl Catal A-Gen* 275: 127–139.
6. Boronat M, Illas F, Corma A (2009) Active sites for H_2 adsorption and activation in Au/TiO_2 and the role of the support. *J Phys Chem A* 113: 3750–3757.
7. Bus E, Miller JT, van Bokhoven JA (2005) Hydrogen chemisorption on Al_2O_3-supported gold catalysts. *J Phys Chem B* 109: 14581–14587.
8. Caballero C, Valencia J, Barrera M, et al. (2010) Selective hydrogenation of citral over gold nanoparticles on alumina. *Powder Technol* 203: 412–414.
9. Campo B, Ivanova S, Gigola C, et al. (2008) Crotonaldehyde hydrogenation on supported gold catalysts. *Catal Today* 133: 661–666.
10. Cárdenas-Lizana F, Gomez-Quero S, Baddeley CJ, et al. (2010) Tunable gas phase hydrogenation of m-dinitrobenzene over alumina supported Au and Au–Ni. *Appl Catal A-Gen* 387: 155–165.
11. Cárdenas-Lizana F, Gomez-Quero S, Keane MA (2008) Ultra-selective gas phase catalytic hydrogenation of aromatic nitro compounds over Au/Al_2O_3. *Catal Commun* 9: 475–481.
12. Cárdenas-Lizana F, Gomez-Quero S, Keane MA (2009) Gas phase hydrogenation of m-dinitrobenzene over alumina supported Au and Au–Ni alloy. *Catal Lett* 127: 25–32.
13. Cárdenas-Lizana F, Gomez-Quero S, Keane MA (2008) Exclusive production of chloroaniline from chloronitrobenzene over Au/TiO_2 and Au/Al_2O_3. *ChemSusChem* 1: 215–221.
14. Cárdenas-Lizana F, Keane MA (2013) The development of gold catalysts for use in hydrogenation reactions. *J Mater Sci* 48: 543–564.
15. Claus P (2005) Heterogeneously catalysed hydrogenation using gold catalysts. *Appl Catal A-Gen* 291: 222–229.
16. Claus P, Brückner A, Mohr C, et al. (2000) Supported gold nanoparticles from quantum dot to mesoscopic size scale: effect of electronic and structural properties on catalytic hydrogenation of conjugated functional groups. *J Am Chem Soc* 122: 11430–11439.
17. Chambers RP, Boudart M (1966) Selectivity of gold for hydrogenation and dehydrogenation of cyclohexene. *J Catal* 5: 517–528.
18. Chen YW, Lee DS (2013) Liquid phase hydrogenation of p-chloronitrobenzene on $Au–Pd/TiO_2$ catalysts: effects of reduction method. *Mod Res Catal* 2: 25–34.
19. Choudhary TV, Sivadinarayana C, Datye AK, et al. (2003) Acetylene hydrogenation on Au-based catalysts. *Catal Lett* 86: 1−8.
20. Corma A, Boronat M, González S, et al. (2007) On the activation of molecular hydrogen by gold: a theoretical approximation to the nature of potential active sites. *Chem Commun* 3371–3373.
21. Díaz G, Antonio GC, Orlando HC, et al. (2011) Hydrogenation of citral over $IrAu/TiO_2$ catalysts. effect of the preparation method. *Top Catal* 54: 467–473.
22. Fujitani T, Nakamura I, Akita T, et al. (2009) Hydrogen dissociation by gold clusters. *Angew Chem Int Ed* 48: 9515–9518.
23. Gomez S, Torres C, Luis JGF, et al. (2012) Hydrogenation of nitrobenzene on Au/ZrO_2 catalysts. *J Chil Chem Soc* 57: 1194–1198.
24. Guan Y, Hensen EJM (2009) Cyanide leaching of Au/CeO_2: highly active gold clusters for 1,3-butadiene hydrogenation. *Phys Chem Chem Phys* 11: 9578–9582.

25. Hartfelder U, Kartusch C, Makosch M, et al. (2013) Particle size and support effects in hydrogenation over supported gold catalysts. *Catal Sci Technol* 3: 454–461.
26. Hashmi ASK (2007) Gold-catalyzed organic reactions. *Chem Rev* 107: 3180–3211.
27. Hugon A, Delannoy L, Louis C (2008) Supported gold catalysts for selective hydrogenation of 1,3-butadiene in the presence of an excess of alkenes. *Gold Bull* 41: 127–138.
28. Jia J, Haraki K, Kondo JN, et al. (2000) Selective hydrogenation of acetylene over Au/Al_2O_3 catalyst. *J Phys Chem B* 104: 11153–11156.
29. Milone C, Crisafulli C, Ingoglia R, et al. (2007) A comparative study on the selective hydrogenation of α,β-unsaturated aldehyde and ketone to unsaturated alcohols on Au supported catalysts. *Catal Today* 122: 341–351.
30. Milone C, Ingoglia R, Schipilliti L, et al. (2005) Selective hydrogenation of α,β-unsaturated ketone to α,β-unsaturated alcohol on gold-supported iron oxide catalysts: role of the support. *J Catal* 236: 80–90.
31. Cárdenas-Lizana F, Gomez-Quero S, Hugon A, et al. (2009) Pd-promoted selective gas phase hydrogenation of p-chloronitrobenzene over alumina supported Au. *J Catal* 262: 235–243.
32. Zhang X, Shi H, Xu BQ (2005) Catalysis by gold: isolated surface Au^{3+} ions are active sites for selective hydrogenation of 1,3-butadiene over Au/ZrO_2 catalysts. *Angew Chem Int Ed* 44: 7132–7135.
33. Corma A, Garcia H (2008) Supported gold nanoparticles as catalysts for organic reactions. *Chem Soc Rev* 37: 2096–2126.
34. Mohr C, Hofmeister H, Claus P (2003) The influence of real structure of gold catalysts in the partial hydrogenation of acrolein. *J Catal* 213: 86–94.
35. Mohr C, Hofmeister H, Radnik J, et al. (2003) Identification of active sites in gold-catalyzed hydrogenation of acrolein. *J Am Chem Soc* 125: 1905–1911.
36. Stobinski L, Zommer L, Dus R (1999) Molecular hydrogen interactions with discontinuous and continuous thin gold films. *Appl Surf Sci* 141: 319–325.
37. Boronat M, Concepcion P, Corma A (2009) Unravelling the nature of gold surface sites by combining IR spectroscopy and DFT calculations. Implications in catalysis. *J Phys Chem C* 113: 16772–16784.
38. Nikolaev SA, Smirnov VV (2009) Synergistic and size effects in selective hydrogenation of alkynes on gold nanocomposites. *Catal Today* 147: S336–S341.
39. Nikolaev SA, Permyakov NA, Smirnov VV, et al. (2010) Selective hydrogenation of phenylacetylene into styrene on gold nanoparticles. *Kinet Catal* 51: 288–292.
40. Guo X, Liu Q, Wang L, et al. (2012) Synthesis, morphology and optical properties of multi-pods Au/FeO(OH) and Au/Fe_2O_3 nanostructures. *Mater Sci Eng B-Adv* 177: 321–326.
41. Radnik J, Mohr C, Claus P (2003) On the origin of binding energy shifts of core levels of supported gold nanoparticles and dependence of pretreatment and material synthesis. *Phys Chem Chem Phys* 5: 172–177.
42. Crook R, Deering J, Fussell SJ, et al. (2010) Enhance reactivity of silver- and gold-catalysted hydrogenations using silver(I) salts. *Tetrahedron Lett* 51: 5181–5184.
43. Edwards JK, Solsona BE, Landon P, et al. (2005) Direct synthesis of hydrogen peroxide from H_2 and O_2 using TiO_2-supported Au–Pd catalysts. *J Catal* 236: 69–79.

44. Liao S, Yu Z, Xu Y, et al. (1995) A remarkable synergic effect of polymer-anchored bimetallic palladium-ruthenium catalysts in the selective hydrogenation of p-chloronitrobenzene. *J Chem Soc Chem Commun* 1155–1156.
45. Hosseini M, Siffert S, Tidahy HL, et al. (2007) Promotional effect of gold added to palladium supported on a new mesoporous TiO_2 for total oxidation of volatile organic compounds. *Catal Today* 122: 391–396.
46. Nutt MO, Heck KN, Alvarez P, et al. (2006) Improved Pd-on-Au bimetallic nanoparticle catalysts for aqueous-phase trichloroethene hydrodechlorination. *Appl Catal B-Environ* 69: 115–125.
47. Nutt MO, Hughes JB, Wong MS (2005) Designing Pd-on-Au bimetallic nanoparticle catalysts for trichloroethene hydrodechlorination. *Environ Sci Technol* 39: 1346–1353.
48. Vasil'kov AY, Nikolaev SA, Smirnov VV, et al. (2007) An XPS study of the synergetic effect of gold and nickel supported on SiO_2 in the catalytic isomerization of allylbenzene. *Mendeleev Commun* 17: 268–270.
49. Venezia AM, La Parola V, Deganello G, et al. (2003) Synergetic effect of gold in Au/Pd catalysts during hydrodesulfurization reactions of model compounds. *J Catal* 215: 317–325.
50. Piccinini M, Edwin NN, Edwards JK, et al. (2010) Effect of reaction conditions on the performance of Au–Pd/TiO_2 catalyst for the direct synthesis of hydrogen peroxide. *Phys Chem Chem Phys* 12: 2488–2492.
51. Rousset JL, Cadete-Santos-Aires FJ, Sekhar BR, et al. (2000) Comparative X-ray photoemission spectroscopy study of Au, Ni, and AuNi clusters produced by laser vaporization of bulk metals. *J Phys Chem B* 104: 5430–5435.
52. Yuan G, Louis C, Delannoy L, et al. (2007) Silica- and titania-supported Ni–Au: application in catalytic hydrodechlorination. *J Catal* 247: 256–268.
53. Wu Z, Zhao Z, Zhang M (2010) Synthesis by replacement reaction and application of TiO_2-supported Au–Ni bimetallic catalyst. *ChemCatChem* 2: 1606–1614.
54. Liu YC, Huang CY, Chen YW (2006) Hydrogenation of p-chloronitrobenzene on Ni–B nanometal catalysts. *J Nanopart Res* 8: 223–230.
55. Liu YC, Huang CY, Chen YW (2006) Liquid-phase selective hydrogenation of p-chloronitrobenzene on Ni–P–B nanocatalysts. *Ind Eng Chem Res* 45: 62−69.
56. Wang X, Perret N, Delgado JJ, et al. (2013) Reducible support effects in the gas phase hydrogenation of p-chloronitrobenzene over gold. *J Phys Chem C* 117: 994–1005.
57. Yan X, Liu M, Liu H, et al. (2001) Role of boron species in the hydrogenation of o-chloronitrobenzene over polymer-stabilized ruthenium colloidal catalysts. *J Mol Catal A-Chem* 169: 225–233.
58. Chen YW, Lee DS, Chen HJ (2012) Preferential oxidation of CO in H_2 stream on Au/ZnO–TiO_2 cataalysts. *Int J Hydrogen Energ* 37: 15140–15155.
59. Sandoval A, Aguilar A, Louis C, et al. (2011) Bimetallic Au–Ag/TiO_2 catalyst prepared by deposition-precipitation: high activity and stability in CO oxidation. *J Catal* 281: 40–49.
60. Sarkany A, Geszti O, Safran G (2008) Preparation of Pd shell–Au core/SiO_2 catalyst and catalytic activity for acetylene hydrogenation. *Appl Catal A-Gen* 350: 157–163.
61. Sarkany A, Horvath A, Beck A (2002) Hydrogenation of acetylene over low Loaded Pd and Pd–Au/SiO_2 catalysts. *Appl Catal A-Gen* 229: 117–125.
62. Serna P, Concepción P, Corma A (2009) Design of highly active and chemoselective bimetallic gold–platinum hydrogenation catalysts through kinetic and isotopic studies. *J Catal* 265: 19–25.

63. Stakheev AY, Kustov LM (1999) Effects of the support on the morphology and electronic properties of supported metal clusters: modern concepts and progress in 1990s. *Appl Catal A-Gen* 188: 3–35.
64. Steiner P, Hüfner S (1981) Core level binding energy shifts in Ni on Au and Au on Ni overlayers. *Solid State Commun* 37: 279–283.
65. Zafeiratos S, Kennou S (2001) Photoelectron spectroscopy study of surface alloying in the Au/Ni (s) 5(0 0 1) × (1 1 1) system. *Appl Surf Sci* 173: 69–75.

AIMS Press